Wide-Area Measurement-Based Stabilizing Control of Power System Considering Signal Transmission Delay

Balarko Chaudhuri, *Student Member, IEEE*, Rajat Majumder, *Student Member, IEEE*, and Bikash C. Pal, *Senior Member, IEEE*

***Abstract*—Recent technological advances in the area of wide-area measurement systems (WAMS) has enabled the use of a combination of measured signals from remote locations for centralized control purpose. The transmitted signals can be used for multiple swing mode damping using a single controller. However, there is an unavoidable delay involved before these signals are received at the controller site. To ensure satisfactory performance, this delay needs to be taken into account in the control design stage. This paper focuses on damping control design taking into account a delayed arrival of feedback signals. A predictor-based $\mathcal{H}_\infty$ control design strategy is discussed for such time-delayed systems. The concept is utilized to design a WAMS-based damping controller for a prototype power system using a static var compensator. The controller performance is evaluated for a range of operating conditions.**

***Index Terms*—H-infinity control, inter-area oscillations, LMI, model reduction, remote signals, robustness, Smith predictor, swing mode.**

I. Introduction

IN A PRACTICAL power system, the number of dominant inter-area modes is often larger than the number of controllable devices available to control them. Research attention, therefore, has been focused on designing new control structures to improve the damping of multiple swing modes. The primary idea behind the control design is to employ a combination of remote stabilizing signals with diverse modal contents [1].

With rapid advancements in WAMS technology, the transmission of measured signals to remote control center has become relatively simpler. This has made the prospect of damping of inter-area oscillations through remote measurements a realistic one. From an economic viewpoint, implementation of the centralized control using remote signals often turns out to be more cost effective than installing new control devices [1]. The obvious question is how fast are these remote measurements available to the control site. Employing phasor measurement units (PMU), it is possible to deliver the signals at a speed of as high as 30 Hz sampling rate [2], [3]. It is possible to deploy the PMUs at strategic locations of the grid and obtain a coherent picture of the entire network in real time [3].

Manuscript received December 5, 2003. This work was supported by the ABB (U.S.) and EPSRC (U.K.) under Grant GR/R/31676. Paper no. TPWRS-00592-2003.

The authors are with the Department of Electrical and Electronic Engineering, Imperial College London, London SW7 2BT, U.K. (e-mail: b.chaudhuri@imperial.ac.uk; r.majumder@imperial.ac.uk; b.pal@imperial.ac.uk).

Digital Object Identifier 10.1109/TPWRS.2004.835669

However, the cost and associated complexities restrict the use of such sophisticated signal transmission hardware in a large commercial scale. As a more viable alternative, the existing communication channels are often used to transmit signals from remote locations. The major problem is the delay involved between the instant of measurement and that of the signal being available to the controller. This delay can typically be in the range of 0.5–1.0 s, depending on the distance, protocol of transmission and several other factors. As the delay is comparable to the time periods of some of the critical inter-area modes, it should be accounted for in the design stage itself to ensure satisfactory control action. Our previous work [4] has illustrated a $\mathcal{H}_\infty$-based centralized control design methodology without considering the delay (0.02–0.05 s) involved in transmitting the remote signals. In that case, the delay was much less than the lowest time period of the inter-area modes and therefore we could ignore it in the design stage.

In this work, the power system is treated as a dead-time system involving a delay in transmitting the measured signals from remote locations to the controller site. It is very difficult to control such time-delayed systems [5]. Smith predictor (SP) [6], [7] approach, proposed in the early fifties, is the first effective tool for handling such control problems. $\mathcal{H}_\infty$ controllers are not likely to guarantee satisfactory control action for time-delayed systems. The difficulties associated with the design of $\mathcal{H}_\infty$ controllers for such systems and the potential solution using the predictor-based approach is discussed in details in Section III.

One of the drawbacks of the classical Smith predictor (CSP) approach is that it is very difficult to ensure a minimum damping ratio of the closed loop poles when the open-loop plant has lightly damped poles (as often encountered in power systems). A modified Smith predictor (MSP) approach, proposed by Wantanable *et al.* [8], can be used to overcome the drawbacks of the CSP. However, the control design using MSP approach might run into numerical problems for systems with fast stable poles. To overcome the drawbacks of CSP and MSP, an unified Smith predictor (USP) approach was proposed very recently by Zhong [9]. The USP approach effectively combines the advantageous features of both the CSP and MSP.

Therefore, an USP approach is adopted in this work to formulate the damping control design problem for a power system having a signal transmission delay of 0.75 s. A $\mathcal{H}_\infty$ controller is designed by solving the problem using linear matrix inequalities (LMIs) with additional pole-placement constraints. The methodology is demonstrated by designing a 2-input, 1-output

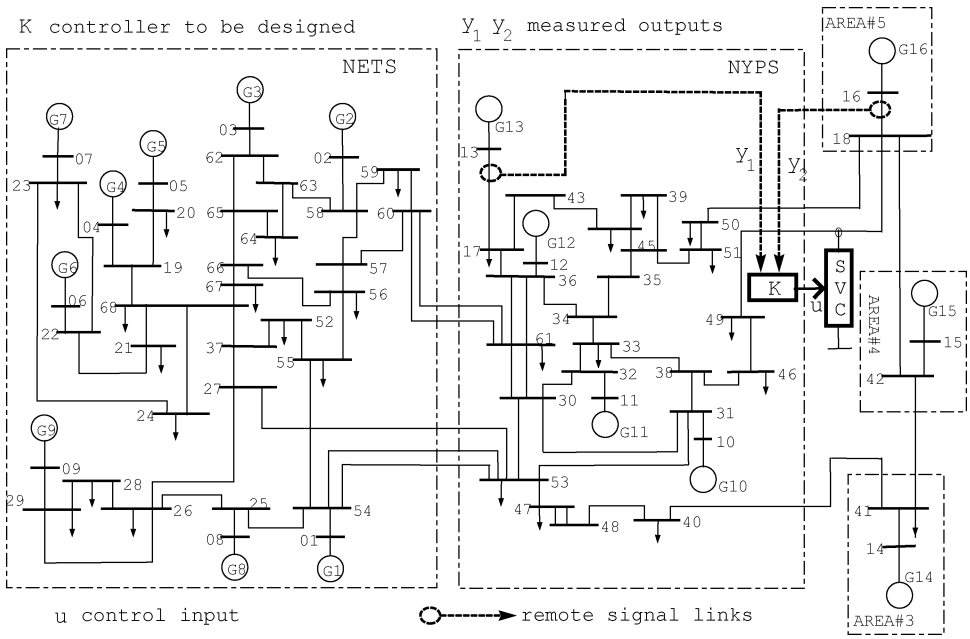

Fig. 1. The 16-machine, 68-bus study system with SVC.

damping controller for a SVC installed in a 16-machine, 68-bus prototype power system. The performance and robustness of the designed controller is verified using eigenvalue analysis and time domain simulations.

II. Study System

A 16-machine, 68-bus study system, shown in Fig. 1, was considered for this study. The detailed description of the study system including network data and dynamic data for the generators, excitation systems, PSSs can be found in [10] and [11].

An SVC is installed in the middle of the tie-line connecting NYPS with area #5 to improve the voltage profile of the system. The topology of the SVC is assumed to have a thyristor controlled reactor (TCR) of 150 MVAr capacity in parallel with a fixed capacitor (FC) of 200 MVAr. At 1.0 pu voltage, this corresponds to a susceptance range of -1.50 to 2.0 pu, which sets the limits of the SVC output. The steady-state settings of the FC and the TCR are 150 MVAr and 33 MVAr, respectively. Under nominal operating condition, the tie-line power flow from NYPS to NETS is 700 MW.

The small-signal dynamic model of the SVC is shown in Fig. 2, where $T_{\rm svc}$ is the response time of the thyristor control circuitry, T_m is the time constant involved with the voltage measurement hardware, and T_{v1} and T_{v2} are the time constants of the voltage regulator block.

The machine, exciter, network power flow and SVC models are linearized about the nominal operating condition in order to obtain the system matrix.

The eigenvalues of the system, displayed in Table I, confirm the presence of four inter-area modes out of which the first three are critical necessitating damping control action.

Mode #4 on its own settles in less than 10 s as its frequency (0.79 Hz) is comparatively higher than the other modes (the higher the oscillation frequency, the faster is the settling for a given damping ratio). Since the influence of this mode on

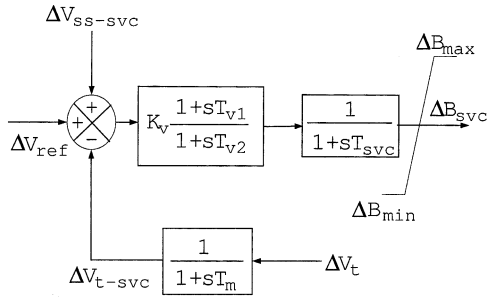

Fig. 2. Small-signal dynamic model of SVC.

TABLE I
Inter-Area Modes of the Study System

ζ	f (Hz)
0.0635	0.3853
0.0432	0.5039
0.0558	0.6204
0.0499	0.7913

inter-area oscillation does not last beyond 10 s and an overall system settling time of 10–12 s is acceptable, it is not required to provide additional damping to this mode. Therefore, it was decided to provide supplementary damping control action for the first three critical inter-area modes only.

A modal observability analysis [12] was carried out to identify the most effective stabilizing signals for each of these modes. The results of the observability analysis revealed that $P_{13,17}$ is most effective for modes #1 and #3 and $P_{16,18}$ for mode #2, where $P_{13,17}$ and $P_{16,18}$ indicate the power-flow in the lines between buses #13–#17 and buses #16–#18, respectively.

Depending on the distance of the measurement site and the mode of signal transmission, a time-delay typically in the range of 0.01 s to 1.0 s can be expected in practice. In this paper, a time-delay of 0.75 s is considered to illustrate the control design exercise.

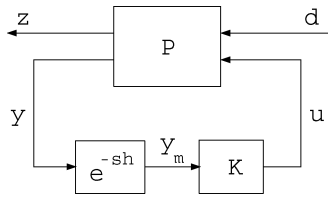

Fig. 3. Control setup for dead-time systems.

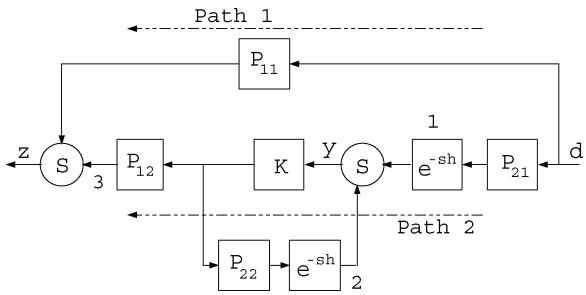

Fig. 4. Equivalent representation of dead-time systems.

III. Smith Predictor for Dead-Time Systems: An Overview

In a dead-time system, either the measured output takes certain time before it affects the control input or the action of the control input takes certain time before it influences the measured outputs. Typical dead-time systems consist of input and/or output delays. The general control setup for a system having an output delay is shown in Fig. 3, where

$$P(s) = \begin{bmatrix} P_{11}(s) & P_{12}(s) \\ P_{21}(s) & P_{22}(s) \end{bmatrix}. \tag{1}$$

The closed-loop transfer matrix from d to z is: $T_{zd}(s) = P_{11} + P_{12}Ke^{-sh}(I - P_{22}Ke^{-sh})^{-1}P_{21}$. This suggests that an instantaneous response exists through the path P_{11} (path 1 in Fig. 4) without any delay. An equivalent structure is shown in Fig. 4.

It can be seen that during the period $t = 0 \sim h$ after d is applied, the output z is not controllable, since it is only determined by P_{11} and d with no response coming through the controlled path (path 2 in Fig. 4). This means that the $\mathcal{H}_\infty$ performance index $\|T_{zd}\|_\infty$ is likely to be dominated by a response that can not be controlled which is not desirable. It is extremely difficult to design a controller for such systems [5].

A Smith predictor (SP), as mentioned before, is the first effective tool for tackling such control problems. The primary idea is to eliminate any uncontrollable response that is likely to govern the $\mathcal{H}_\infty$ performance index. One possible way of achieving this is to introduce an uniform delay in both the paths (path 1 and path 2), as shown in Fig. 6. There are two steps toward achieving this. First, the delay blocks (e^{-sh}) at points 1 and 2 need to be shifted to point 3 by introducing a suitable predictor block in parallel with K. Second, a delay block needs to be introduced in path 1.

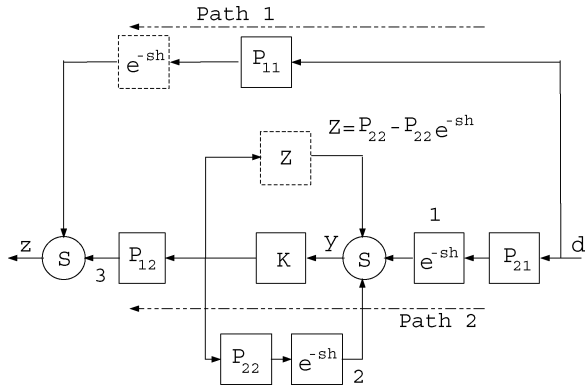

Fig. 5. Introduction of SP and delay block.

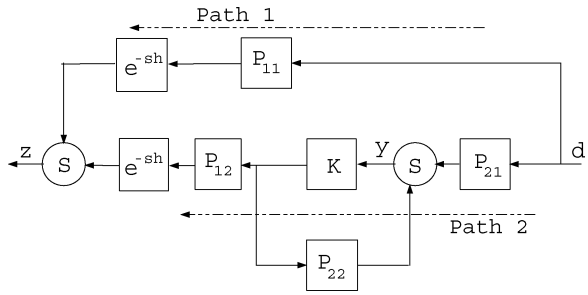

Fig. 6. Uniform delay in both paths.

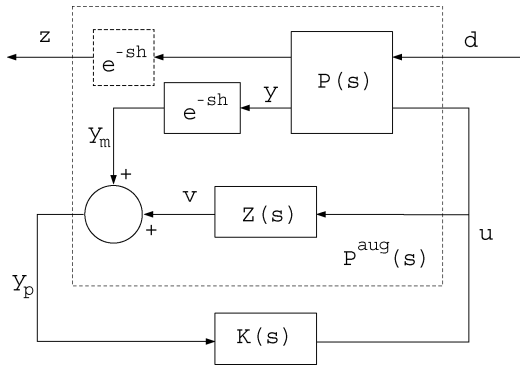

Fig. 7. Smith Predictor formulation.

The first step is achieved by introducing a SP block $Z(s) = P_{22}(s) - P_{22}(s)e^{-sh}$, as shown by the dotted box in Fig. 5. The second task of bringing a delay in path 1 is done while forming the generalized plant prior to control design. Presence of the predictor block Z and the delay in path 1 ensures that the responses (through path 1 and path 2) governing the performance index is delayed uniformly as shown in Fig. 6.

A predictor-based controller for the dead-time plant $P_h(s) = P_{22}(s)e^{-sh}$ consists of a predictor $Z = P_{22} - P_{22}e^{-sh}$ and a stabilizing compensator K, as shown in Fig. 7. The predictor Z is an exponentially stable system such that $P_h + Z$ is rational i.e. it does not involve any uncontrollable response governing the $\mathcal{H}_\infty$ performance index.

To overcome the shortcomings of the CSP approach for plants having poorly damped open-loop poles, the MSP approach was introduced which enabled the robust control problems of dead-

time systems to be solved similarly as in the finite dimensional situations [5]. Let us consider a generalized delay-free plant given by

$$P(s) = \left[\begin{array}{c|cc} A & B_1 & B_2 \\ \hline C_1 & D_{11} & D_{12} \\ C_2 & D_{21} & D_{22} \end{array}\right] = \begin{bmatrix} P_{11} & P_{12} \\ P_{21} & P_{22} \end{bmatrix}. \quad (2)$$

For a delay of h, the generalized plant formulation using the MSP approach would be [5]

$$\tilde{P}(s) = \left[\begin{array}{c|cc} A & e^{Ah}B_1 & B_2 \\ \hline C_1 & 0 & D_{12} \\ C_2e^{-Ah} & D_{21} & 0 \end{array}\right]. \quad (3)$$

The computation of matrix exponential e^{-Ah} in (3) suffers from numerical problems especially for systems having fast stable eigenvalues. In the worst case, it might well be noncomputable. This problem can even arise with reasonably small amount of delays if some of the stable eigenvalues are very fast.

In $\mathcal{H}_\infty$, mixed-sensitivity formulation for power system damping control design, the presence of fast stable eigenvalues in the augmented plant cannot be ruled out, the possible sources being the fast sensing circuits ($T \sim 0.02\,\mathrm{s}$), fast damper circuits ($T \sim 0.05$ s), and even the weighting filters. These often lead to numerical instability while solving the problem using LMIs. These problems are overcome through the use of the USP [9] formulation. This is achieved by decomposing the delay free plant P into a critical part P_c and a noncritical part P_{nc}. The critical part contains the poorly damped poles of the system whereas, the noncritical part consists of poles with sufficiently large negative real values. Section IVdescribes the generalized problem formulation using this approach.

IV. Problem Formulation Using Unified Smith Predictor

As indicated in Section III, the first step toward formulating the control problem using the USP approach is to decompose the delay-free plant into critical and noncritical parts. This is normally done by applying a suitable linear coordinate transformation on the state-space representation of the plant. In this work, a suitable transformation matrix V was chosen such that the transformed matrix $J = V^{-1}AV$ is in the Jordan canonical form which is free from complex entries. The transformation matrix V was chosen using the "*eig*" function available in Matlab [13]. The elements of the transformed matrix J were converted from complex diagonal form to a real diagonal form using the "*cdf2rdf*" function in Matlab [13]. The transformed augmented delay-free plant P_{22}^t is given by

$$P_{22}^t(s) = \left[\begin{array}{c|c} V^{-1}AV & V^{-1}B_2 \\ \hline C_2V & D_{22} \end{array}\right] = \left[\begin{array}{cc|c} A_c & 0 & B_c \\ 0 & A_{nc} & B_{nc} \\ \hline C_c & C_{nc} & D_{22} \end{array}\right] \quad (4)$$

where A_c is critical and A_{nc} is the noncritical part of A. The augmented plant P_{22}^t can be split as $P_{22}^t = P_c + P_{nc}$, where

$$P_c(s) = \left[\begin{array}{c|c} A_c & B_c \\ \hline C_c & D_{22} \end{array}\right] \quad (5)$$

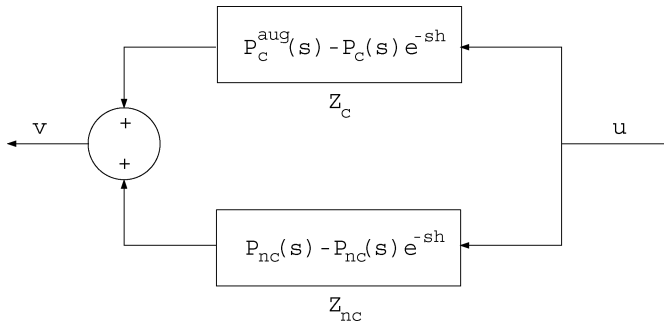

Fig. 8. Unified SP.

and

$$P_{nc}(s) = \left[\begin{array}{c|c} A_{nc} & B_{nc} \\ \hline C_{nc} & 0 \end{array}\right] \quad (6)$$

The predictor for the critical part is formulated using the MSP approach by applying a completion operator [5]. On a rational transfer matrix $G(s) = D + C(sI - A)^{-1}B$, the completion operator $\pi_h\{e^{-sh}G\}$ is defined as follows:

$$\pi_h\{e^{-sh}G\} = \left[\begin{array}{c|c} A & B \\ \hline Ce^{-Ah} & 0 \end{array}\right] - \left[\begin{array}{c|c} A & B \\ \hline C & D \end{array}\right] e^{-sh}. \quad (7)$$

Using (7), the predictor for the critical part P_c is given by (8) (see [5] for details)

$$\begin{aligned} Z_c(s) &= \pi_h\{e^{-sh}P_c\} \\ &= \left[\begin{array}{c|c} A & B_c \\ \hline C_ce^{-A_ch} & 0 \end{array}\right] - \left[\begin{array}{c|c} A_c & B_c \\ \hline C_c & D_c \end{array}\right] e^{-sh} \\ &= P_c^{aug}(s) - P_c(s)e^{-sh}. \end{aligned} \quad (8)$$

The predictor for the noncritical part is constructed following the CSP formulation and is given by

$$Z_{nc}(s) = P_{nc}(s) - P_{nc}(s)e^{-sh}. \quad (9)$$

The USP, denoted by Z, is simply the sum of Z_c and Z_{nc}, as shown in Fig. 8.

It is given by

$$Z(s) = P_{22}^{aug}(s) - P_{22}^t(s)e^{-sh} \quad (10)$$

where $P_{22}^{aug} = P_{nc} + P_c^{aug}$. Using (4), (6) and (8), the realization for P_{22}^{aug} can be expressed in the form

$$P_{22}^{aug} = \left[\begin{array}{c|c} A & B_2 \\ \hline C_2E_h & 0 \end{array}\right] \quad (11)$$

where

$$E_h = V \begin{bmatrix} e^{-A_ch} & 0 \\ 0 & I_{nc} \end{bmatrix} V^{-1}. \quad (12)$$

The augmented plant P^{aug} is obtained by connecting the original dead-time plant and the USP in parallel—see Fig. 7, where the new set of measured outputs are y_p. The expression for P^{aug} is given by

$$P^{aug} = \begin{bmatrix} P_{11}(s) & P_{12}(s)e^{-sh} \\ P_{21}(s) & P_{22}(s)^{aug} \end{bmatrix}. \quad (13)$$

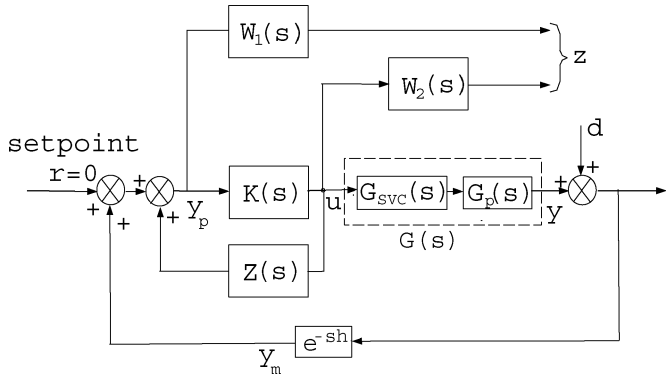

Fig. 9. Control setup with mixed-sensitivity design formulation.

The generalized plant $\tilde{P}$ can be formulated from P^{aug} after inserting the delay block e^{-sh} in between d and z, as shown by a dotted box in Fig. 7. The steps for arriving at the final expression for $\tilde{P}$ is detailed in [9] and is not presented here due to space restrictions. The final form of the generalized plant is the following:

$$\tilde{P}=\left[\begin{array}{cc|cc} A & 0 & E_h^{-1}B_1 & B_2 \\ 0 & A_{nc} & [0\ \ e^{A_{nc}h}-I_{nc}]V^{-1}B_1 & 0 \\ \hline C_1 & C_1V\begin{bmatrix}0\\ I_{nc}\end{bmatrix} & 0 & D_{12} \\ C_2E_h & 0 & D_{21} & 0 \end{array}\right]. \tag{14}$$

Having formulated the generalized plant $\tilde{P}$ following the USP approach, the objective is to design a controller K to meet the desired performance specifications. If K ensures the desired performance for $\tilde{P}$, then controller predictor combination $K_e = K(I - ZK)^{-1}$ is guaranteed to achieve the same for the original dead-time plant [5].

V. Control Design

The control design problem was formulated using the standard mixed-sensitivity approach [4], [14] with modifications described in the earlier sections. The overall control setup is shown in Fig. 9, where $G_p(s)$ is the power system model, $G_{svc}(s)$ is the SVC model, $W_1(s), W_2(s)$ are the weighting filters, $K(s)$ is the controller to be designed, $Z(s)$ is the SP, d is the disturbance at the plant output, z is the weighted exogenous output, y_m is the measured output, and u is the control input. In the context of our problem, y_m represents the remote measurements $P_{13,17}$ and $P_{16,18}$ and u represents the supplementary control input to the SVC which corresponds to ΔV_{ss-svc} in Fig. 2. The design objective is the following: find a controller K from the set of internally stabilizing controllers $\mathbb{S}$ such that

$$\min_{K\in\mathbb{S}} \left\| \begin{bmatrix} W_1S \\ W_2KS \end{bmatrix} \right\|_\infty < 1 \tag{15}$$

where $S = (I - GK)^{-1}$ is the sensitivity. The solution to the problem was sought numerically using LMI solver with additional pole-placement constraint. Once the generalized plant is formulated following the steps mentioned in Section IV, the basic steps for control design are similar to those outlined in [14] and are summarized below.

1) Reduce the plant size.

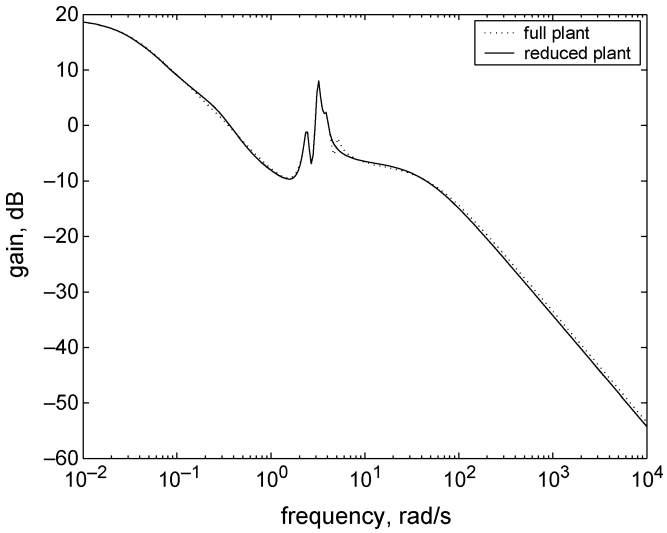

Fig. 10. Frequency response of the full and reduced plant.

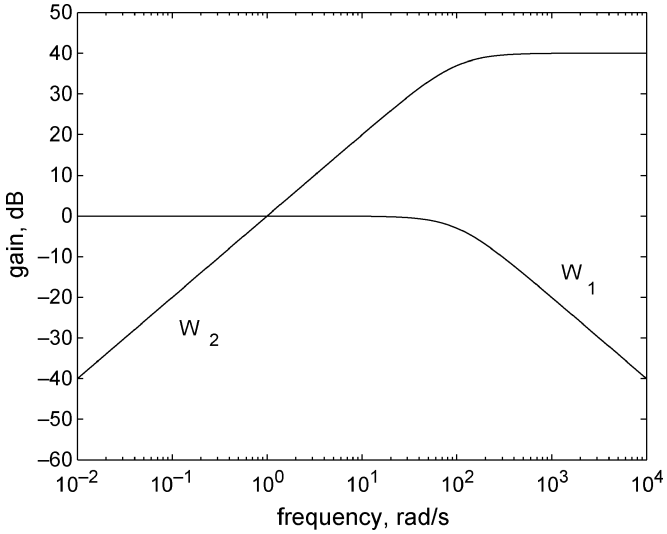

Fig. 11. Frequency response of the weighting filters.

2) Formulate the generalized plant using the reduced plant and the mixed-sensitivity weights.
3) Design the controller using the *LMI Toolbox* with additional pole-placement constraints.
4) Reduce the designed controller size.
4) Test the reduced controller on the full-order (real) plant with appropriate delays.

The 134th-order open-loop plant was approximated to a tenth-order equivalent, as shown in Fig. 10.

The weights were chosen as follows:

$$W_1(s) = \frac{100}{s+100}, \quad W_2(s) = \frac{100s}{s+100}. \tag{16}$$

The frequency responses for the weighting filters are shown in Fig. 11. They are in accordance with the basic requirement of mixed-sensitivity design, i.e., $W_1(s)$ should be a low-pass filter for output disturbance rejection and $W_2(s)$ should be a high-pass filter in order to reduce the control effort and to ensure robustness against additive uncertainties in the plant model in the high-frequency range.

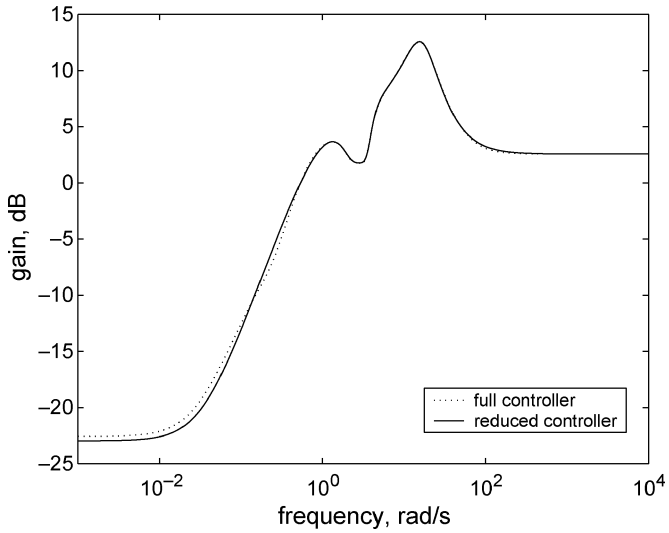

Fig. 12. Frequency response of the full and reduced controller.

Using the reduced plant model and the above mentioned weights, the generalized problem was formulated according to (14). The solution was numerically sought using suitably defined objectives in the argument of the function *hinfmix* of the *LMI Toolbox* in Matlab [13]. The pole-placement constraint was imposed by using a "conic sector" of inner angle $2cos^{-1}(0.175)$ and apex at the origin. The order of the controller obtained from the LMI solution was equal to the reduced-order augmented plant order plus the order of the weights. The designed controller was reduced to a tenth-order equivalent using Schur's method without affecting the frequency response, as shown in Fig. 12.

The state-space representation of the 2-input, 1-output controller is given in Appendix I.

The measured signals were fed to the controller through a washout filter $10s/(10s+1)$ in each channel. This prevents the damping controller from responding to steady changes in power flow. It is a standard practice to include the washout circuit in order to prevent the damping controllers from responding to very slow variations in the system conditions [15]. A limit was also imposed on the controller output to comply with the voltage response specification of the SVC.

VI. Performance Evaluation and Robustness Validation

An eigenvalue analysis of the closed-loop system was carried out to examine the performance of the designed controller in terms of improving the damping ratios of the inter-area modes. A fourth-order Pade approximation was used to represent the delay in the frequency domain. The results are summarized in Table II. It can be seen that the damping ratios of the three critical inter-area modes, shown in boldface, are improved in the presence of the controller.

The damping action of the controller was examined under different power flow levels to validate its robustness. Table III displays the results when the power flow from NETS to NYPS varies in the range of 100–900 MW. The damping is found to be highly satisfactory over this range of power-flow variation.

TABLE II
Damping Ratios and Frequencies of the Inter-Area Modes

Mode no.	No control		With control	
	ζ	f (Hz)	ζ	f (Hz)
1	0.0635	0.3853	**0.1340**	0.4027
2	0.0432	0.5039	**0.1718**	0.5119
3	0.0558	0.6204	**0.1514**	0.7072
4	0.0499	0.7913	0.0665	0.8066

TABLE III
Damping Ratios and Frequencies of the Critical Inter-Area Modes at Different Levels of Power Flow Between NETS and NYPS

Power flow (MW)	Mode 1		Mode 2		Mode 3	
	ζ	f(Hz)	ζ	f(Hz)	ζ	f(Hz)
100	**0.1077**	0.4128	**0.2019**	0.5220	**0.1338**	0.6931
500	**0.1249**	0.4076	**0.1866**	0.5142	**0.1461**	0.7018
700	**0.1340**	0.4027	**0.1718**	0.51197	**0.1514**	0.7072
900	**0.1410**	0.3959	**0.1514**	0.5105	**0.1555**	0.7132

TABLE IV
Damping Ratios and Frequencies of the Critical Inter-Area Modes for Different Load Models

Load model	Mode 1		Mode 2		Mode 3	
	ζ	f(Hz)	ζ	f(Hz)	ζ	f(Hz)
CI	**0.1340**	0.4027	**0.1718**	0.51197	**0.1514**	0.7072
CC+CI	**0.1169**	0.4011	**0.1393**	0.5193	**0.1385**	0.7501
CP+CI	**0.1123**	0.3984	**0.1219**	0.5260	**0.1705**	0.6030
Dynamic	**0.1368**	0.3960	**0.1783**	0.5290	**0.1521**	0.7072

TABLE V
Damping Ratios and Frequencies of the Critical Inter-Area Modes for Different Tie-Line Strengths

Outage of tie-line	Mode 1		Mode 2		Mode 3	
	ζ	f(Hz)	ζ	f(Hz)	ζ	f(Hz)
60-61	**0.1338**	0.3726	**0.0968**	0.5066	**0.1914**	0.6936
53-54	**0.1357**	0.3697	**0.1160**	0.5113	**0.1831**	0.6917
27-53	**0.1410**	0.3928	**0.1555**	0.5113	**0.1638**	0.7005

The performance of the controller was further evaluated with various load models including constant impedance (CI), a mixture of constant current and constant impedance (CC+CI), a mixture of constant power and constant impedance (CP+CI) and dynamic load characteristics. The dynamic load (induction motor type) was considered at bus #41, the remaining being of CI type. It is evident from the results of Table IV that the designed controller provides robust damping for different load characteristics.

Table V demonstrates the performance robustness following outage of different tie-lines connecting NETS and NYPS. The damping action is found to be satisfactory following the outage of each of the tie-lines connecting buses #27–#53, buses #60–#61, and buses #53–#54.

The damping performance of the designed controller was therefore found to be robust against widely varying operating conditions.

VII. Simulation Results

A large disturbance was simulated by creating a 3-phase line to ground fault at bus #53 followed by tripping one of the lines connecting buses #53 and #54. A time-domain simulation was

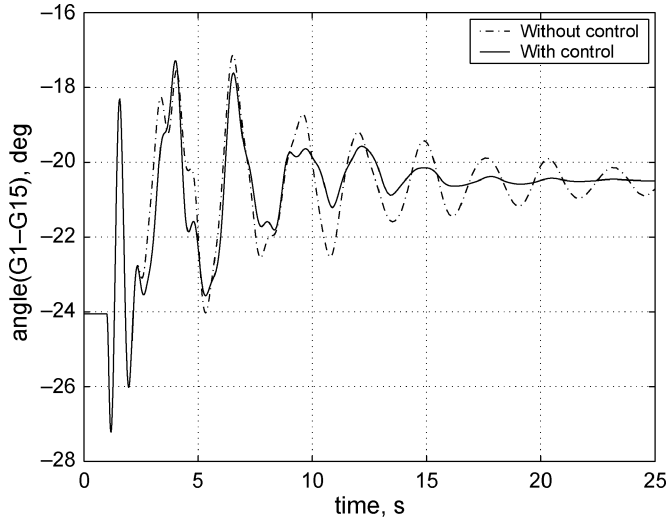

Fig. 13. Dynamic response of the system; controller designed considering delay.

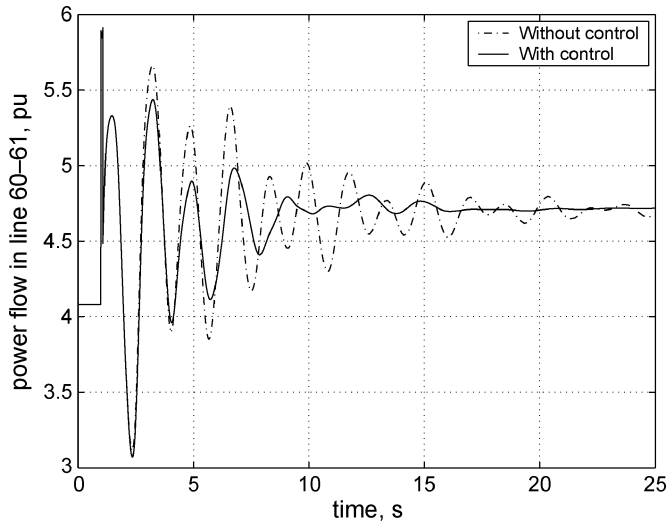

Fig. 14. Power flow in the tie-line 60–61; controller designed considering delay.

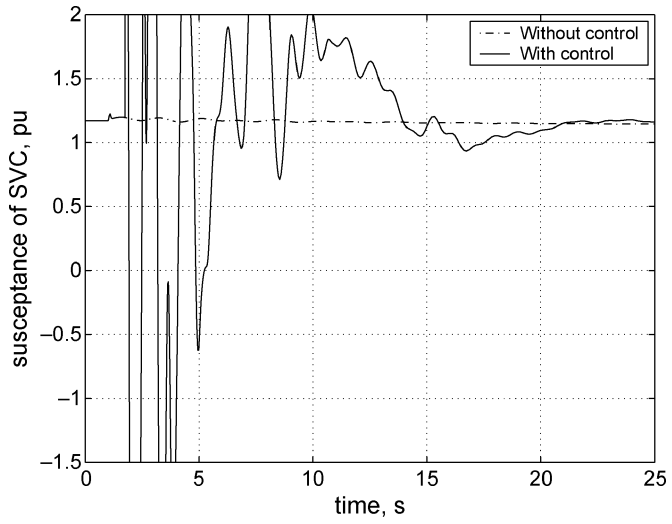

Fig. 15. Output of the SVC.

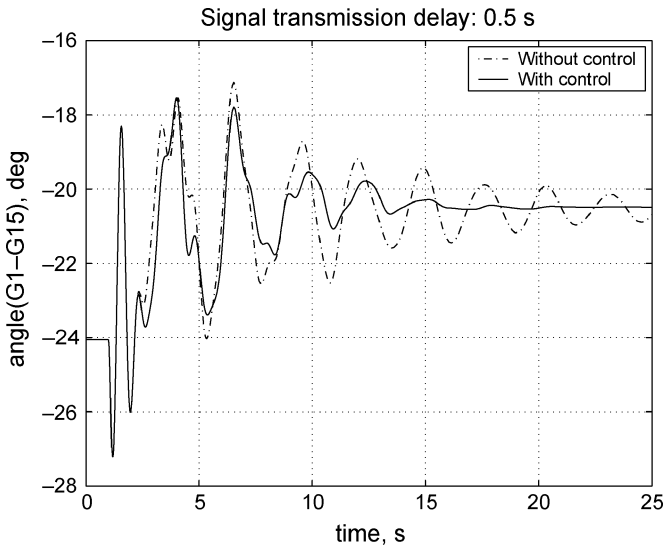

Fig. 16. Dynamic response of the system with a delay of 0.5 s.

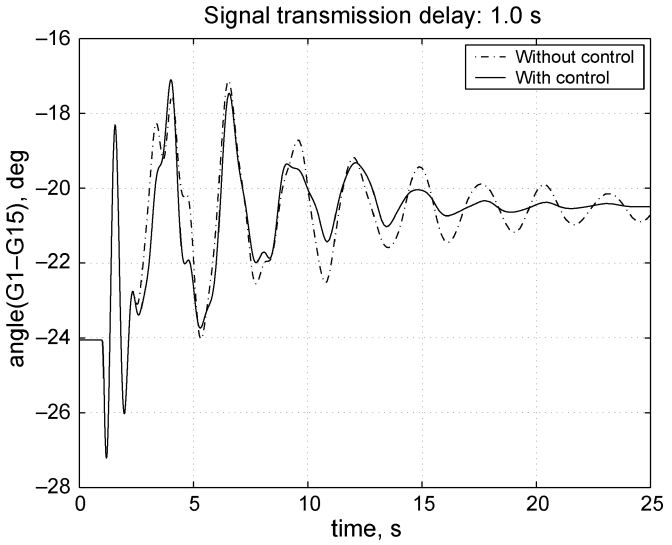

Fig. 17. Dynamic response of the system with a delay of 1.0 s.

carried out in *Simulink* for 25 s, employing the *trapezoidal* method with a variable step size. The "transport delay" blocks in *Simulink* were used to simulate the signal transmission delays and also to implement the USP. The dynamic response of the system following this disturbance is shown in Fig. 13 which exhibits the relative angular separation between the generators G1 and G15, which are located in separate geographical regions. It is clear that the inter-area oscillation is damped out in 12–15 s, even though the feedback signals arrive at the control location after a finite time delay of 0.75 s.

The variation in power flow in the tie-line connecting buses #60–#61 is shown in Fig. 14. It can be seen that the oscillations in tie-line power flow settle within 12–15 s in the presence of the designed controller and predictor combination.

The output variation of the SVC is shown in Fig. 15, which is within the range of -1.5 to 2.0 pu.

Although the controller is designed considering a delay of 0.75 s, there can always be some variation in the amount of delay that is actually encountered in practice. The designed controller

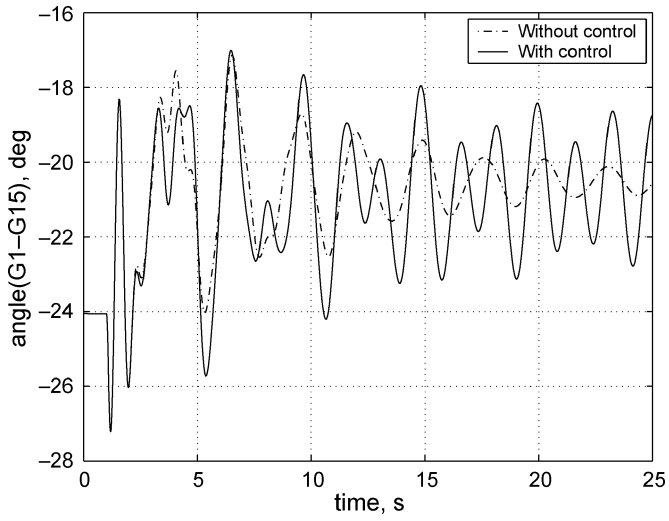

Fig. 18. Dynamic response of the system; controller designed without considering delay.

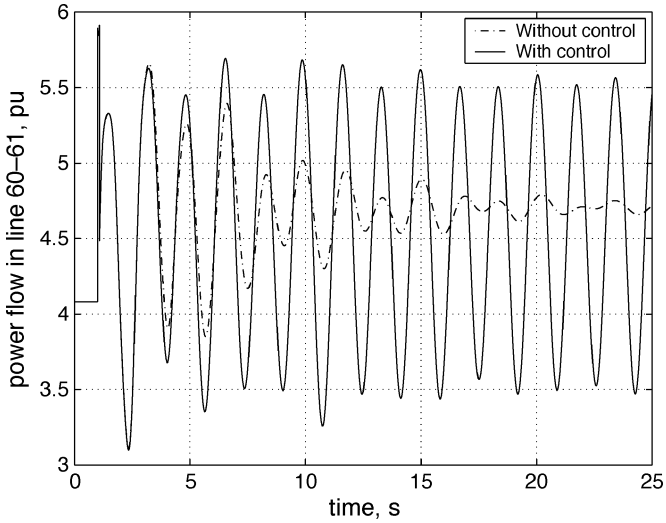

Fig. 19. Power flow in the tie-line 60–61; controller designed without considering delay.

is therefore tested for a range of delays. It has been found that below 0.5 and above 1.0 s delay, the performance deteriorates. Over the range of 0.5 to 1.0 s delay, the controller performs satisfactorily as shown in Figs. 16 and 17.

To demonstrate the drawback of the conventional $\mathcal{H}_\infty$ design with a delay-free plant, a separate controller was designed for the SVC without considering any delay at the design stage. The design was carried out following the LMI-based methodology described in [4], [14]. The controller performed satisfactorily both in time and frequency domain for delays up to 0.1 s. For larger time delays, the performance of the controller appeared to be poor and was even worse with increasing amount of delay. Simulations were carried out with this controller considering a time delay of 0.75 s. The simulation results following the same disturbance described above are shown in Figs. 18 and 19.

It is clear that the system performance deteriorates considerably revealing the fact that if the delay is more than the time-period corresponding to the dominant modes and it is not taken into account during the design stage the controller might not perform as expected. Therefore, it is necessary to include the delay in the control design formulation itself. The results demonstrate a potential application of the USP approach for power system damping control design involving a finite amount of signal transmission delay.

VIII. Conclusion

This paper presents a methodology for power system damping control design accounting for delayed arrival of feedback signals from remote locations. A predictor-based $\mathcal{H}_\infty$ control design strategy is discussed for such a time-delayed system. The design procedure based on the USP approach has been applied for centralized design of power system damping controller through an SVC. A combination of the USP and the designed controller is found to work satisfactorily under different operating scenarios even though the stabilizing signals could reach the controller site only after a finite time.

In this paper, a fixed time delay has been considered for all the communication channels. In practice, this might not always be the case as the distance of the measurement sites differs. Depending on that, different amount of delays for each signal need to be considered during the design. We would like to continue our research in that direction.

$$A = 1 \times 10^4 \times \begin{bmatrix} -10\,137 & 91.3060 & 7.8215 & -7.1367 & 29.2910 & 0.3072 & -9.1325 & 2.9884 \\ 92.2790 & -0.8317 & -0.0711 & 0.0646 & -0.2663 & -0.0028 & 0.0836 & -0.0284 \\ 2.8178 & -0.0248 & -0.0026 & 0.0022 & -0.0086 & 1.5650 \times 10^{-4} & 0.0023 & 0.0010 \\ -5.4397 & 0.0492 & 0.0040 & -0.0039 & 0.0157 & 2.2243 \times 10^{-4} & -0.0049 & 0.0017 \\ 23.0970 & -0.2080 & -0.0178 & 0.0164 & -0.0669 & -6.1045 \times 10^{-4} & 0.0206 & -0.0055 \\ 2.3191 & -0.0215 & -0.0018 & 0.0013 & -0.0065 & -1.8726 \times 10^{-4} & 0.0022 & -0.0015 \\ -11.1780 & 0.1005 & 0.0085 & -0.0076 & 0.0324 & 5.1795 \times 10^{-4} & -0.0103 & 0.0035 \\ 1.2070 & -0.0105 & -0.0014 & 4.4658 \times 10^{-4} & -0.0039 & -9.6293 \times 10^{-5} & 9.8730 \times 10^{-4} & -8.9845 \times 10^{-4} \end{bmatrix}$$

$$B = \begin{bmatrix} -1.0126 \times 10^5 & 875.8100 & 66.8590 & -71.0510 & 265.9700 & -7.3959 & -94.7540 & -2.1494 \\ 2.7738 \times 10^4 & -261.0900 & 4.7133 & 15.1510 & -52.6720 & -13.7650 & 28.2220 & 19.6040 \end{bmatrix}^T$$

$$C = [-1299 \quad 11.5170 \quad 1.4201 \quad -0.6772 \quad 4.0094 \quad 0.0195 \quad -1.1818 \quad -0.0760]$$

APPENDIX I
CONTROLLER STATE-SPACE REPRESENTATION

The state-space representation of the 2-input, 1-output centralized controller for the SVC is given in the equation at the bottom of the previous page.

ACKNOWLEDGMENT

The authors gratefully acknowledge the ideas and suggestions received from Dr. Q. C. Zhong, Dr. I. M. Jaimoukha, and Dr. T. C. Green during this research.

REFERENCES

[1] J. Chow, J. Sanchez-Gasca, H. Ren, and S. Wang, "Power system damping controller design using multiple input signals," *IEEE Control Syst. Mag.*, vol. 20, pp. 82–90, Aug. 2000.
[2] I. Kamwa, R. Grondin, and V. Hebert, "Wide-area measurement based stabilizing control of large power systems—A decentralizedlhierarchical approach," *IEEE Trans. Power Syst.*, vol. 16, pp. 136–153, Feb. 2001.
[3] G. Heydt, C. Lin, A. Phadke, and V. Vittal, "Solutions for the crisis in electric power supply," *IEEE Comput. Appl. Power*, vol. 14, pp. 22–30, July 2001.
[4] B. Chaudhuri and B. Pal, "Robust damping of multiple swing modes employing global stabilizing signals with a TCSC," *IEEE Trans. Power Syst.*, vol. 19, pp. 499–506, Feb. 2004.
[5] Q. C. Zhong, "H_∞ control of dead time systems based on a transformation," *Automatica*, vol. 39, pp. 361–366, Feb. 2003.
[6] O. Smith, "Closer control of loops with dead time," *Chem. Eng. Prog.*, vol. 53, no. 5, pp. 217–219, 1957.
[7] ——, *Feedback Control Systems*. New York: McGraw-Hill, 1958.
[8] K. Wantanable and M. Ito, "A process-model control for linear systems with delay," *IEEE Trans. Automat. Contr.*, vol. AC-26, pp. 1261–1269, Dec. 1981.
[9] Q.-C. Zhong and G. Weiss. (2003) A onified Smith predictor based on the spectral decomposition of the plant. *Automatica* [Online] Available at http://www.ee.ic.ac.uk/CAP/Reporls/2003.html
[10] B. Pal, A. Coonick, and B. Coty, "Robust damping of interarea oscillations in power systems with superconducting magnetic energy storage devices," *Proc. Inst. Elect. Eng. Generation Transmission and Distribution*, vol. 146, no. 06, pp. 633–639, Nov. 1999.
[11] G. Rogers, *Power System Oscillations*. Norwell, MA: Kluwer, 2000.
[12] N. Martins and L. Lima, "Determination of suitable locations for power system stabilizers and static var compensators for damping electromechanical oscillations in large power systems," *IEEE Trans. Power Syst.*, vol. 5, pp. 1455–1469, Nov. 1990.
[13] *Matlab Users Guide*, The Math Works, Inc., Natick, MA, 1998.
[14] B. Chaudhuri, B. Pal, A. C. Zolotas, I. M. Jaimoukha, and T. C. Green, "Mixed-sensitivity approach to H_∞ control of power system oscillations employing multiple facts devices," *IEEE Trans. Power Syst.*, vol. 18, pp. 1149–1156, Aug. 2003.
[15] P. Kundur, *Power System Stability and Control*. New York: McGraw-Hill, 1994.

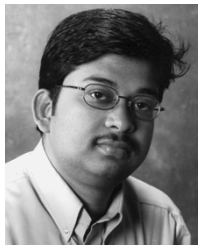

Balarko Chaudhuri (S'04) received the B.E.E. (Hons.) degree from Jadavpur University, Calcutta, India, and the M.Tech from the Indian Institute of Technology, Kanpur, India, in 2000 and 2002, respectively. He is currently pursuing the Ph.D. degree in the Control and Power Group at Imperial College London, London, U.K.

Rajat Majumder (S'04) received the B.E.E. (Hons.) degree from Jadavpur University, Calcutta, India, and the M.Sc. (Engg.) degree from the Indian Institute of Science, Bangalore, India, in 2000 and 2003, respectively. He is currently pursuing the Ph.D. degree in the Control and Power Group at Imperial College London, London, U.K.

Bikash C. Pal (M'00–SM' 03) received the B.E.E. (Hons.) degree from Jadavpur University, Calcutta, India, and the M.E. degree from the Indian Institute of Science, Bangalore, India, in 1990 and 1992, respectively. He received the Ph.D. degree from Imperial College London, London, U.K., in 1999.

He is presently a Lecturer in the Department of Electrical and Electronic Engineering, Imperial College London. His research interests are in the area of power system dynamics and FACTS controllers.